

Reverse Calibration Method for Welding Spots Based on PD/PS Simulation System

Yuan Li, Haibo Xu, Pengjie Wei, Kailin Wang, Yanbing Hu, Kang Zhu, Jun Zhou, Yang Zhang Zhejiang Geely Run Automobile Co., Ltd. Ningbo Hangzhou Bay Branch, Hangzhou, China

Abstract: To address the persistent positional mismatches between simulated welding point coordinates and the actual locations of robotic equipment encountered in automotive body shop production lines, this paper introduces a novel reverse calibration methodology for welding spot trajectories. The approach is implemented within the established Process Designer/Process Simulate (PD/PS) simulation environment. Conventional methods in robot program reverse export result in significant deviations, making them inadequate to meet engineering precision requirements. This study aims to bridge this technical gap. Our solution involves the development of a dedicated RobotTool plugin. Leveraging this empirical data, a sophisticated spatial geometric transformation model is constructed. Through this model, the key transformation matrix describing the relationship between the theoretical simulation coordinate system and the actual physical coordinate system is solved. To improve calibration accuracy and enhance robustness against measurement noise, the least squares optimization algorithm is introduced in conjunction with a specifically designed error optimization function. This mechanism effectively filters high-precision inlier data points, thereby establishing a robust deviation compensation model. Comprehensive experimental validation conducted on representative production setups demonstrates the efficacy of the proposed method. It successfully achieves reverse correction of both welding points and their interconnecting trajectories, consistently controlling positional errors within a stringent tolerance of ±10mm. Crucially, for retrofit and production line upgrade projects, this method allows legacy vehicle welding programs to be directly output as production-ready, zero-debugging industrial robot code following the calibration process. This capability drastically reduces the traditionally intensive on-site commissioning workload by over 80%, thereby significantly enhancing operational efficiency and accelerating the deployment cycles for flexible manufacturing systems handling multiple vehicle models.

Keywords: Welding spot Trajectories; PD/PS Platform; Least Squares Optimization; Automotive Body Shop; Industrial Robot

1. Introduction

With the escalating demand for manufacturing flexibility within the automotive sector, production lines are increasingly required to handle multiple vehicle models concurrently. When introducing new models or implementing line modifications or upgrades to enhance throughput, the robot programs utilized on the physical production floor must be imported into simulation environments for theoretical validation and verification. However, persistent positional discrepancies exist between the theoretical coordinates defined in the simulation models and the actual positions

measured on-site. These deviations primarily stem from cumulative machining inaccuracies, fixture assembly tolerances, and equipment installation variances. Consequently, robot programs exported directly from the physical production line cannot be seamlessly applied within the theoretical simulation environment without significant adaptation. This necessitates labor-intensive, time-consuming, and error-prone manual correction of robot paths by engineers directly on the shop floor—a process characterized by its inefficiency, computational complexity, and inherent risk of introducing errors, thereby compromising overall production efficiency.

To effectively resolve these critical challenges, this paper presents a novel reverse calibration methodology specifically designed for welding spot trajectories. Its core technical innovations encompass three key aspects: (1) The development and implementation of a bespoke RobotTool plugin within the established PD/PS simulation platform. This plugin facilitates the precise, real-time mapping and alignment of actual physical shop-floor robot trajectories with their corresponding theoretical counterparts in the simulation environment. (2) The formulation of a robust error compensation model, incorporating a dual-threshold constraint mechanism, which rigorously filters data and optimizes parameters to guarantee exceptionally high calibration fidelity. (3) The capability for reverse correction of legacy welding programs. This pivotal feature enables the direct adaptation of existing, historically deployed programs using the derived calibration parameters, thereby drastically diminishing the requirement for repetitive, labor-intensive on-site debugging operations [1-3].

2. Theoretical Model for Robot Position Calibration

2.1 Transformation Model Construction Principle

Assuming a spatial point P has coordinates P^r in the theoretical simulation coordinate system and Pt in the actual coordinate system, ignoring robot posture and tool TCP influence, they satisfy the spatial geometric transformation relationship:

$$P^t = RP^r + T \tag{1}$$

where R is the rotation matrix and T is the translation vector.

Combining R and T into a homogeneous transformation matrix:

$$\begin{bmatrix} P^t \\ 1 \end{bmatrix} = \begin{bmatrix} R & T \\ 0 & 1 \end{bmatrix} \begin{bmatrix} P^r \\ 1 \end{bmatrix} \tag{2}$$

Expanded form:

$$\begin{bmatrix} P_x^t \\ P_y^t \\ P_z^t \\ 1 \end{bmatrix} = \begin{bmatrix} n_x & o_x & a_x & T_x \\ n_y & o_y & a_y & T_y \\ n_z & o_z & a_z & T_z \\ 0 & 0 & 0 & 1 \end{bmatrix} \begin{bmatrix} P_x^r \\ P_y^r \\ P_z^r \\ 1 \end{bmatrix}$$
(3)

Here, the homogeneous transformation matrix $\begin{bmatrix} R & T \\ 0 & 1 \end{bmatrix}$ represents the mapping function f from

the theoretical to the actual coordinate system. Its 12 elements constitute the model's unknown parameters. Expanding the system of equations via matrix multiplication:

$$n_{x}P_{x}^{r} + o_{x}P_{y}^{r} + a_{x}P_{z}^{r} + T_{x} = P_{x}^{t}$$

$$n_{y}P_{x}^{r} + o_{y}P_{y}^{r} + a_{y}P_{z}^{r} + T_{y} = P_{y}^{t}$$

$$n_{z}P_{x}^{r} + o_{z}P_{y}^{r} + a_{z}P_{z}^{r} + T_{z} = P_{z}^{t}$$

$$(4)$$

Analysis shows each equation contains 4 independent unknown parameters (corresponding to base vector components of R and translation components). Solving the complete 12-parameter

transformation model theoretically requires coordinates from at least 4 sampled points.

2.2 Model Parameter Solving Method

In engineering practice, large sample sizes are used for fitting to improve accuracy and applicability, transforming Eq. (3) into an overdetermined system. High-precision measurement data yields a transformation model approximating the real physical space, aiming for compatibility with all data points. However, measurement errors are inevitable. When data doesn't strictly satisfy the ideal model, an optimal approximation model is constructed based on the principle of minimizing error—specifically, minimizing the sum of squared residuals between model predictions and sample points.

Rewriting Eq. (3) in matrix form: AX = B

$$\begin{bmatrix} P_{x1}^{r} & P_{y1}^{r} & P_{z1}^{r} & 1 \\ P_{x2}^{r} & P_{y2}^{r} & P_{z2}^{r} & 1 \\ P_{xi}^{r} & P_{yi}^{r} & P_{zi}^{r} & 1 \\ \vdots & \vdots & \vdots & \vdots \\ P_{xn}^{r} & P_{yn}^{r} & P_{zn}^{r} & 1 \end{bmatrix} \begin{bmatrix} n_{x} & n_{y} & n_{z} \\ o_{x} & o_{y} & o_{z} \\ a_{x} & a_{y} & a_{z} \\ T_{x} & T_{y} & T_{z} \end{bmatrix} = \begin{bmatrix} P_{x1}^{t} & P_{y1}^{t} & P_{z1}^{t} \\ P_{x2}^{t} & P_{y2}^{t} & P_{z2}^{t} \\ P_{xi}^{t} & P_{yi}^{t} & P_{zi}^{t} \\ \vdots & \vdots & \vdots \\ P_{xn}^{r} & P_{yn}^{r} & P_{zn}^{r} \end{bmatrix}$$
(5)

where i = 1, 2, 3, ..., n denotes the sample point index and $n \ge 4$. When n = 4, Eq. (5) yields a determined solution; when $n \ge 4$, it is overdetermined. To minimize residuals between the transformation model and measurement points, the least squares solution is used:

$$X = (A^T A)^{-1} A^T B \tag{6}$$

where $Xx = [nx \ ox \ ax \ Tx]T$, $Xy = [ny \ oy \ ay \ Ty]T$, $Xz = [nz \ oz \ az \ Tz]T$ are solved independently. Note: Different numbers or spatial distributions of test points yield different solutions (excluding overfitting risks). Additionally, since the rotation matrix R = [noa] must satisfy the orthogonality constraint RTR = I [4], this condition must be enforced during solving to ensure theoretical validity.

2.3 Theoretical Model Error Analysis

Solving the transformation f from theoretical to actual coordinates via least squares requires at least 4 sample points. Randomly select N sample points $Pn(n \ge 4)$ to form the model point set M for parameter solving. After obtaining f, the model's generalization ability is validated. Remove the selected N points from theoretical set B and actual set T to form validation sets $BC = \{p | p \in B \setminus M\}$ and $TC = \{p | p \in T \setminus M\}$. Inlier Identification: calculate:

$$\Delta_{i} = \max\{ |\mathbf{p}_{xi}^{A} - \mathbf{p}_{xi}^{T^{c}}|, |\mathbf{p}_{yi}^{A} - \mathbf{p}_{yi}^{T^{c}}|, |\mathbf{p}_{zi}^{A} - \mathbf{p}_{zi}^{T^{c}}| \}$$
 (7)

If $\Delta_i < \tau$ (τ is a preset threshold), classify it as an inlier and add to inlier set I.

Model Validity Screening: If $|I| > N_{min}(N_{min}$ is a size threshold), accept the transformation model.

Optimal Model Selection: If multiple valid models are generated iteratively, evaluate them using the inlier residual variance function:

$$Dn = \frac{1}{|I| - 1} \sum_{1}^{|I|} (\Delta i - \overline{\Delta})^2, \qquad \overline{\Delta} = \frac{1}{|I|} \sum_{1}^{|I|} \Delta i$$
 (8)

Select the model with the smallest D_n as the optimal solution [5-6]. This process enhances model robustness and accuracy by eliminating outliers.

3. Implementation via Secondary Development

3.1 System Feasibility

Siemens Tecnomatix Process Designer & Process Simulate (PD/PS) is an integrated digital manufacturing platform developed by Siemens Digital Industries Software [7-9], widely used in process planning, robot programming, and virtual commissioning. Its secondary development system supports deep functional extensions via COM/.NET API interfaces, meeting the high-precision process simulation needs of discrete manufacturing (automotive, aerospace, etc.) [10]. This system develops a welding spot calibration module based on this architecture (see Figures 3 & 4), utilizing PD/PS's process object modeling kernel and kinematics simulation engine for precise robot pose mapping. PD/Ps platform provides a reserved interface class the TxButtonCommand, which enables direct invocation of internal PD/PS APIs. This class is an inheritable type that requires a minimum the overriding of the Category, Name, and Execute functions. Core implementation logic is typically written within the Execute function. This study employs Visual Studio 2022 as the development environment, utilizing the Siemens development library the dll file to implement calibration -related methods.

Figure 1 illustrates the workflow of the RobotTool plugin designed to analyze and correct deviations between theoretical and actual weld point coordinates during robotic welding. Key stages include: data import involving acquiring theoretical coordinates from simulation platforms (PD/PS) and actual coordinates from on-site measurement equipment; application of a spatial geometric transformation model to map theoretical to physical coordinate systems; generation of a relative deviation matrix containing rotation/translation parameters defining coordinate system mapping; error assessment for each data point; automated outlier detection removing points exceeding preset thresholds (e.g., ±10mm) to enhance calibration accuracy and robustness; reverse calibration applying optimized transformation parameters to valid field data after deviation matrix solution and outlier filtering; and final output of corrected welding trajectory data or robot control code meeting engineering precision requirements. This process ensures accurate robotic welding path adjustments based on actual measurements, thus improving welding performance and quality.

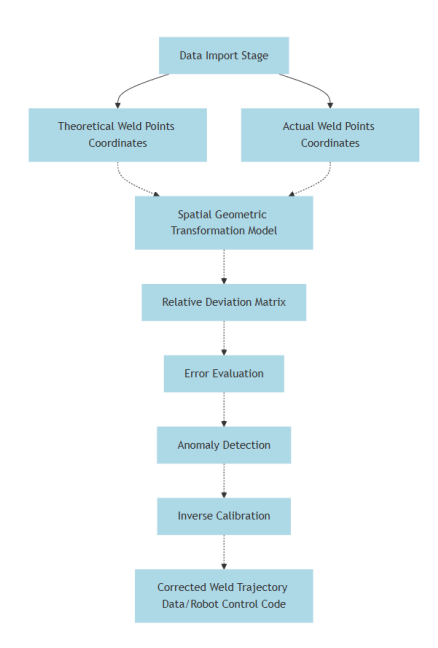


Figure 1: Workflow of RobotTool Plugin for Calibration.

3.2 System Workflow

To comprehensively evaluate the effectiveness of the weld spot reverse calibration method, 14 key weld points from the inner panel assembly line of a vehicle's rear door were selected for experimentation (Table 1), covering high-precision welding areas such as body hinge reinforcement plates and lock striker installation zones, with these weld points exhibiting a three-dimensional curved spatial distribution characterized by a maximum curvature radius of R = 280 mm, while the experimental environment utilized Siemens PDPS 16.1 platform (featuring a compatibility module loaded with the new calibration algorithm) and a KUKA KR210 R2700 extra robot with ± 0.03 mm repeat positioning accuracy and 210 kg payload capacity[11-12].

Table 1: Weld Point Data for Rear Door Assembly (Unit: Mm).

Spot ID	Theoretical Coord (x, y, z)	Actual Coord (x, y, z)	Uncalibrated Error
P02WP1615438	4324.31, 28.43, 1276.51	4257.08, 49.53, 1248.03	74.45
P02WP1615437	4322.70, 98.41, 1276.51	4255.23, 114.52, 1248.16	73.91
P02WP1615436	4319.14, 170.64, 1276.53	4252.13, 184.89, 1248.86	73.02
P02WP1615435	4313.76, 240.44, 1276.54	4246.20, 260.35, 1248.50	74.08
P02WP1615434	4306.86, 306.93, 1276.06	4239.06, 331.98, 1248.27	76.02
P02WP1615429	4324.31, -28.42, 1276.51	4257.75, -12.68, 1251.36	72.58
P02WP1615430	4322.70, -98.40, 1276.51	4256.56, -78.91, 1249.58	74.44
P02WP1615431	4319.14, -170.63, 1276.53	4252.93, -150.92, 1249.72	73.82
P02WP1615432	4313.76, -240.42, 1276.54	4247.77, -217.33, 1249.88	74.01
P02WP1615441	4257.65, -243.95, 1587.09	4190.09, -217.68, 1562.07	77.66
P02WP1615439	4262.80, -176.02, 1588.74	4193.76, -165.34, 1564.44	75.25
P02WP1609707	4264.60, -137.22, 1588.04	4195.78, -123.72, 1565.15	75.29
P02WP1615442	4262.80, 176.03, 1588.74	4195.30, 164.86, 1564.11	74.68
P02WP1609713	4264.60, 137.23, 1588.04	4194.65, 197.62, 1563.47	90.47

Data Import & Preprocessing: Import on-site robot backup programs. Figure 2 shows pink markers for actual welding spots and red markers for theoretical spots, highlighting the deviation. Actual spots exhibit significant deviation within the simulation environment.



Figure 2: Path in Simulation Environment.

User Interaction: Users open the developed software (Figure 3), sequentially add theoretical and on-site reverse-derived welding spots from the simulation software, and check correspondence and counts.

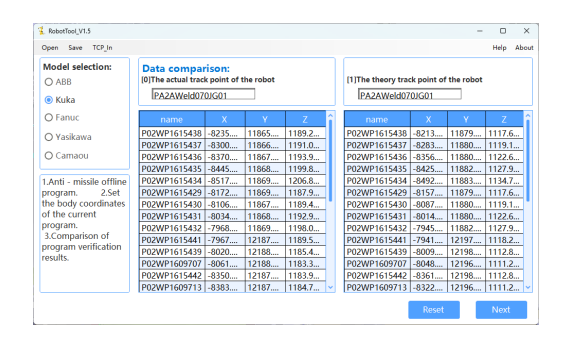




Figure 3: Welding Spot Import Interface.

Figure 4: Welding Spot Error Interface.

Deviation Calculation & Optimization: Using Equation (6), the deviation between theoretical and

optimized points is calculated as:
$$X = \begin{pmatrix} 1 & -0.002 & -0.004 \\ 0.002 & 1 & 0.003 \\ 0.004 & -0.003 & 1 \\ 61.736 & -6.224 & 44.071 \end{pmatrix}$$

Applying Equation (5) yields calibrated coordinates for each weld point (see Table 2). By removing maximum outliers, the overall positional error is controlled within 10 mm. Final deviation is reduced to 8.87 mm through Equation (8).

Table 2: Post-Calibration Data Comparison (Unit: Mm).

Snot ID	Theoretical Count (v. r. z.)	Calibration Count (v. v. v.)	Uncalibrated
Spot ID Theoretical Coord (x, y		Calibration Coord (x, y, z)	Error
P02WP1615438	4324.31, 28.43, 1276.51	4324.14,30.26,1274.24	2.92
P02WP1615437	4322.70, 98.41, 1276.51	4322.44,95.26,1274.59	3.77
P02WP1615436	4319.14, 170.64, 1276.53	4319.49,165.63,1275.52	5.21
P02WP1615435	4313.76, 240.44, 1276.54	4313.72,241.10,1275.43	1.14
P02WP1615434	4306.86, 306.93, 1276.06	4306.72,312.75,1275.47	5.85
P02WP1615429	4324.31, -28.42, 1276.51	4324.69,-31.96,1277.37	4.44
P02WP1615430	4322.70, -98.40, 1276.51	4323.35,-98.18,1275.38	1.38
P02WP1615431	4319.14, -170.63, 1276.53	4319.57,-170.19,1275.30	1.59
P02WP1615432	4313.76, -240.42, 1276.54	4314.27,-236.58,1275.27	5.01
P02WP1615441	4257.65, -243.95, 1587.09	4257.91,-237.82,1587.70	6.15
P02WP1615439	4262.80, -176.02, 1588.74	4261.70,-185.49,1590.22	11.03
P02WP1609707	4264.60, -137.22, 1588.04	4263.81,-143.88,1591.06	7.76
P02WP1615442	4262.80, 176.03, 1588.74	4263.95,144.70,1590.95	31.33
P02WP1609713	4264.60, 137.23, 1588.04	4263.36,177.47,1590.41	42.56

After the calibration work was completed, the calibration effect was verified through practical operation, with the results shown in Figure 5. As can be observed from the figure, the pink weld point coordinates after calibration are largely coincident with the theoretical red coordinates. This indicates that the calibrated weld point positions achieve a high degree of accuracy and that the trajectory

fitting results meet the positional requirements for practical operations. Further, the calibrated trajectory data were imported into the robot control system for actual operation tests. The test results demonstrated smooth and continuous robot movements without encountering any unreachable points or abnormal alarms. This confirms that the current calibration method not only effectively improves the accuracy of weld point coordinates but also ensures the reachability and stability of the robot's motion trajectories. Consequently, it provides reliable technical support for the practical application of subsequent production lines [13].

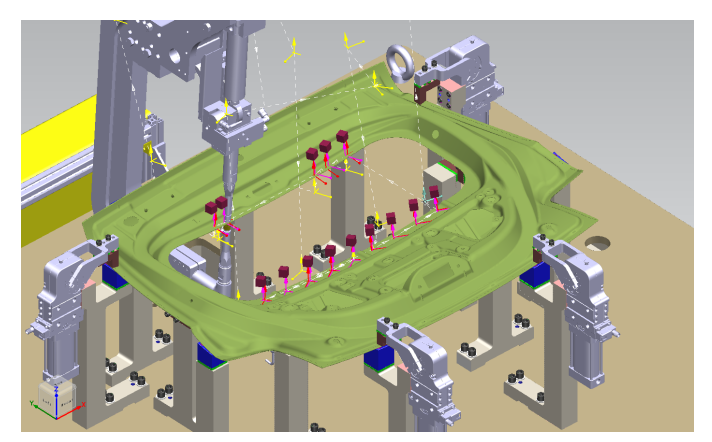


Figure 5: Results After Calibration.

3.3 Engineering Application Value

In the technical upgrading project of a rear door assembly production line for a Geely vehicle model, the application of this weld point inverse teaching calibration method achieved significant improvements in efficiency: compared to traditional approaches, the program migration efficiency improved with the migration time per device reduced from 14 man-days to 2.5 man-days (an 82.1% increase in efficiency). In terms of quality pass rate, the first-piece welding pass rate increased from 63% to 98% (a 55.6 percentage-point reduction in quality defect rate). Regarding safety performance, the average number of collisions per workstation dropped from 7 to 0 (completely eliminating path interference risks). These quantitative data indicate that this method, through precise trajectory mapping and automatic code generation, not only shortens the commissioning cycle by 82%, but also achieves a breakthrough improvement in quality pass rate and fundamental optimization of path safety, providing quantifiable technical support for the flexible transformation of the production line.

4. Conclusion

The reverse calibration method for welding spots proposed in this paper effectively addresses the industry bottleneck of offline trajectory calibration. Key innovations include.

Constructing a spatial transformation model between theoretical (Pr) and actual (Pt) coordinate systems. Developing a RobotTool plugin via PDPS secondary development (COM/.NET API) for real-time mapping of on-site trajectories to simulation trajectories. Solving the overdetermined system (AX=B) using the least squares method, optimizing transformation matrix parameters with threshold constraints $\Delta_i < \tau$ and variance evaluation functions to ensure model robustness and accuracy. Enabling reverse correction of legacy programs, significantly reducing repetitive debugging costs for old model retrofits. Engineering Value Validation: Corrected legacy programs in retrofit projects can directly generate zero-debugging code, reducing on-site workload by 80% and providing an efficient

solution for flexible multi-model production. This method can be extended to other offline programming-dependent industrial scenarios (e.g., laser welding, gluing), offering a theoretical and engineering paradigm for dynamic trajectory calibration within digital twin systems.

References

- [1] International Federation of Robotics, World Robotics Report 2023: Industrial Robots in Automotive Manufacturing. Frankfurt: IFR Press, 2023.
- [2] Y. Zhang et al., "Digital twin-driven calibration for robotic welding systems," Robotics and Computer-Integrated Manufacturing, vol. 71, p. 102167, 2021.
- [3] G. Michalos et al., "Flexible assembly systems reconfiguration planning," CIRP Annals, vol. 69, no. 1, pp. 17–20, 2020.
- [4] P. J. Besl and N. D. McKay, "Method for registration of 3-D shapes," IEEE Trans. Pattern Anal. Mach. Intell., vol. 14, no. 2, pp. 239–256, 1992.
- [5] V. Chebyshev et al., "Robust least squares for industrial robot calibration," Mechanism and Machine Theory, vol. 154, p. 104045, 2020.
- [6] K. Schroer et al., "Error compensation in industrial robots using neural networks," Journal of Manufacturing Systems, vol. 61, pp. 738–752, 2021.
- [7] Siemens Digital Industries Software, Tecnomatix Process Simulate 2206 Developer's Guide. Nuremberg: Siemens AG, 2023.
- [8] T. Kato et al., "Virtual commissioning framework for automotive production lines," IEEE Trans. Ind. Inform., vol. 18, no. 5, pp. 3352–3362, 2022.
- [9] B. Vogel-Heuser et al., "Digital twins in manufacturing: A systematic review," Journal of Industrial Information Integration, vol. 30, p. 100389, 2023.
- [10] M. Bader et al., "Digital twin integration in industrial robotics through secondary development frameworks," Journal of Manufacturing Systems, vol. 62, pp. 567–578, 2022.
- [11] Y. Guo et al., "Outlier rejection strategies in robotic calibration using statistical thresholding," IEEE Transactions on Automation Science and Engineering, vol. 18, no. 3, pp. 1245–1256, 2021.
- [12] A. Patel et al., "High-precision robotic platforms for automotive assembly applications," International Journal of Advanced Manufacturing Technology, vol. 105, no. 9, pp. 3945–3958, 2019.
- [13] J. Wang et al., "Performance evaluation metrics for robot calibration in real-world environments," Robotics and Computer-Integrated Manufacturing, vol. 68, p. 102102, 2021.